Volume 2
Issue 4
December 2013

ISSN 2164-6376 (print)
ISSN 2164-6414 (online)

An Interdisciplinary Journal of

Discontinuity, Nonlinearity, and Complexity

L&H

An Interdisciplinary Journal of

Discontinuity, Nonlinearity, and Complexity

Volume 2, Issue 4, December 2013

L&H Scientific Publishing, LLC, USA

Publication Information

Discontinuity, Nonlinearity, and Complexity (ISSN 2164-6376 (print), eISSN 2164-6414 (online)) is published quarterly (March, June, September, and December) by L & H Scientific Publishing, LLC, P.O. Box 99, Glen Carbon, IL62034, USA. Subscription prices are available upon request from the publisher or from this journal website. Subscriptions are accepted on a prepaid basis only and entered on a calendar year basis. Issues are sent by standard mail (Surface in North America, air delivery outside North America). Priority rates are available upon request. Claims for missing issues should be made within six months of the date of dispatch.

Changes of Address

Send address changes to L&H Scientific Publishing, LLC, P.O. Box 99, Glen Carbon, IL62034, USA. Changes of address must be received at L&H Scientific Publishing eight weeks before they are effective.

Authors Inquiries

For inquiries relative to the submission including electronic submission where available, please visit journal website or contact journal Editors-in-Chief.

Advertising Information

If you are interested in adverting or other commercial opportunities, please email via lhscientificpublishing@gmail.com and your enquiry will be handled as soon as possible.

Printed in USA on acid-free paper.

Discontinuity, Nonlinearity, and Complexity

Continued on back materials

Discontinuity, Nonlinearity, and Complexity 2(4) (2013) 301–319

Discontinuity, Nonlinearity, and Complexity

https://lhscientificpublishing.com/Journals/DNC-Default.aspx

Stochastic Patterns and the Role of Crowding

Claudia Cianci[1] and Duccio Fanelli[2] †

[1]Dipartimento di Sistemi e Informatica, University of Florence and INFN, Via S. Marta 3, 50139 Florence, Italy

[2] Dipartimento di Fisica e Astronomia, University of Florence and INFN, via Sansone 1, Sesto Fiorentino, 50019 Florence, Italy

Submission Info

Communicated by Xavier Leoncini
Received 18 December 2012
Accepted 18 May 2013
Available online 1 January 2014

Keywords

Reaction diffusion equations
Turing and wave instabilities
Molecular Crowding
Stochastic models

Abstract

A stochastic variant of the Brusselator model is investigated. The model accounts for a long range coupling among constituents, as well as for the finite capacity of the embedding medium. The mean field limit of the model is studied and the condition for Turing and wave instability obtained. A degenerate, cusp like transition that separates the domains of Turing and wave order can take place. The point of transition is worked out analytically. Interestingly, the region of Turing instability, as delimited by such transition point, can set in also if the inhibitor diffuses slower then the activator. This is a consequence of the generalized diffusion scheme here analyzed and which originates from having imposed an effect of spatial competition. Beyond the deterministic, mean field picture, we elaborate on the role of stochastic corrections. Granularity, endogenous to the system, can eventually materialize in waves or Turing like patterns, that we here categorized in distinct classes.

1 Introduction

Travelling waves and Turing instability are examples of spatio temporal self-organized patterns [1,2], which can spontaneously emerge in a reaction diffusion scheme. In both cases, a stable homogeneous fixed point can be destabilized by imposing and external, supposedly small, perturbation. Diffusion seeds a linear instability which enhances the aforementioned perturbation. Depending on the specific non linear contributions, and as follows the initial instability, the system under scrutiny can eventually evolve towards distinct asymptotic configurations. Beautiful stationary patterns can for instance materialize, which display rather peculiar topologies, from spirals to stripes. These are the celebrated Turing patterns, recurrently invoked in

†Corresponding author.
Email address: duccio.fanelli@unifi.it

ISSN 2164 – 6376, eISSN 2164 – 6414/$-see front materials © 2013 L&H Scientific Publishing, LLC. All rights reserved.
DOI : 10.5890/DNC.2013.11.001

chemistry [3,4] and biology [1]. Alternatively, and among other possibilities, the density of the constituents can travel through space-time, a phenomenon that is encountered in many contexts of broad applied and fundamental interest.

Reaction-diffusion models are customarily described by resorting to a deterministic approach. The interacting species are organized in families of homologous constituents and their associated concentration is monitored over space and in time. As opposed to this idealised setting, which implies dealing with a system of coupled partial differential equations (PDEs) for the concentration amount, one can adopt an individual based description. The intimate discreteness of the system is thus preserved and stochastic effects are to be accommodated for. The mathematical theory of patterns formation for PDEs of the reaction-diffusion type is well established. Less attention has been instead devoted to characterizing the analogous stochastic frameworks. In a series of recent publications, the effect of the endogenous noise, stemming from finite size fluctuations, was shown to yield to stochastic driven patterns, in a region of the parameters for which macroscopically ordered structures are prevented to occur, according to the deterministic viewpoint. Albeit the dominant deterministic dynamics predicts a stable homogeneous state, the stochastic component can amplify via a resonant mechanism, yielding to stochastic Turing like patterns [5, 7] and/or stochastic waves [6]. It is interesting to emphasize that the impact of finite size fluctuations can be appreciated via direct numerical simulations, but also analytically resolved thanks to an elegant mathematical machinery imported from statistical physics. The van Kampen system size expansion can be in fact applied to quantitatively characterize the deviations from the deterministic dynamics caused by the stochastic effects. This is an approximate technique which enables one to expand the master equation, that rules the underlying stochastic dynamics, by using a measure of the inverse system size as an effective perturbative parameter. At the leading order of the expansion, the deterministic model is obtained, while the next to leading contributions allows one to gain insight into the role played by stochastic fluctuations.

A bottom-up strategy to the modelling, the core of the individual based approach here discussed, can also return mathematical formulations justified from first principle, and different from the heuristically proposed scheme. Emblematic is the case of the reaction/diffusion dynamics of a chemical system made of several species, that are sharing the same spatial reservoir. The diffusion is customarily assumed to be modelled with classical Laplacian terms, as dictated by Fick's law of diffusion. However, when the hosting volume is densely populated, the so called crowding conditions, mutual interferences are present, reflecting excluded volume effects and the competition for spatial microscopic resources. Starting from a correct formulation of the microscopic dynamics and accounting for the finite carrying capacity of the embedding volume, one obtains in fact a modified diffusive behaviour [10], different from that postulated a priori on the basis of a phenomenological ansatz. Cross diffusive terms appear which links multiple diffusing communities and which can contribute to explain the deviation from the conventional Fick's law as seen in crowded molecular diffusion experiments [9]. The interplay between molecular crowding of the type derived in [10] and the Turing instability has been discussed in [8]. According to the conventional Turing scenario, which applies to the diluted limit, the diffusion coefficient of the inhibitor has to be larger than the diffusion coefficient associated to the activator. In short, the system has to accommodate for two competing processes, a short–range activation and long–range inhibition, for the Turing patterns to eventually occur and because of the constraints on the reaction terms, i.e. the stability of the homogeneous, a-spatial, fixed point. At variance, the competition for the available space that materializes in the cross diffusion terms, impacts on the time scales associated to the reactions processes and induces a self–consistent long–range effect that enlarges the region of influence of the inhibitors, also when the diffusion coefficient of the activator is assumed to be faster [8].

Our paper is positioned in this context investigations. We will in particular consider a Brusselator model, with a nonlocal interaction term as hypothesized in [6]. This latter term can be tuned as sought and controls the appearance of travelling wave solutions. Turing instabilities can also develop, for specific parameters setting. At variance with the formulation introduced in [6], we will here impose a finite carrying capacity at the microscopic level, which builds on the general idea of [10], and extends the limit of validity of the model to ideally embrace the regime of crowded conditions. By operating within this setting, we will continue to elaborate on the conditions that yield to the deterministic Turing order, quantifying the role of cross diffusion. Further, the concept of stochastic waves will be revisited working in such a generalized descriptive scenario.

The paper is organized as follows: in the next section the stochastic model is presented and the necessary mathematical concepts introduced. Then, we turn to discussing the mean-field deterministic limit. Under specific conditions, and studying the system in a sub-manifold of reduced dimensionality, a bifurcation is found that separates the region of deterministic Turing and wave instability. The point of bifurcation is determined analytically, a result that casts on solid grounds the observation that Turing order is possible when the activator diffuses faster than the inhibitor, for a generalized reaction-diffusion scheme where cross diffusion terms are accommodated for. Then, in section 4 we turn to discussing the stochastic dynamics. By calculating the power spectrum of fluctuations, we will show that intrinsic noise can trigger time independent Turing patterns and travelling waves, a conclusion that naturally follows from [6,7] and that we here revisit, by including the effects of exclusive interference due to crowding into the model. Finally, in section 5 we sum up and conclude.

2 The stochastic model and its master equation

The system that we are going to study is a modified version of the Brusselator model, with the inclusion of a non local interaction term. This latter contribution was postulated in [6], inspired to previous work [13], and drives a long range correlation in the reaction scheme, which is eventually responsible for the emergence of travelling wave solutions. As compared to the original formulation [6], we will here introduce an additional complication into the model by constraining the number of molecules that can be eventually hosted in a given mesoscopic patch. In doing so, we will force a degree of spatial interference between diffusing species, which indirectly reflects the competition for the available resources.

Imagine the physical space in which the system is embedded to be partitioned in cells (or patch), whose linear size is set to one. Each cell is denoted with a progressive index i. Following [6] we shall assume the number of cells to be infinite, which implies that the underlying space is of infinite extent. Label with X_i (resp. Y_i) a molecule of type X (resp. Y) hosted inside cell i. Moreover, let us call E_i the vacancies, or empty spaces, that are available in patch i. Label with n_i the number of molecules of type X in cell i. Similarly, quantities m_i and q_i refer to species Y and E, respectively. Each cell can then host a maximum of N elements, including the empties, a physical constraint on the local maximal density, which translates into the following mathematical relation:

$$n_i + m_i + q_i = N, \tag{1}$$

N is therefore an invariant quantity of the dynamics which will prove crucial in the forthcoming discussion. The reactions that define the backbone of the models read [6]:

$$\begin{aligned} E_i &\xrightarrow{a} X_i, \\ X_i &\xrightarrow{b} Y_i, \end{aligned} \tag{2}$$

$$2X_i + Y_i \xrightarrow{c} 3X_i,$$
$$X_i \xrightarrow{d} E_i.$$

The quantities a, b, d are scalar parameters and stand for the rates of the associated reactions. The third reaction assumes instead a non local interaction of the type introduced in [6]. More specifically, one imposes a non local coupling which decays exponentially with the distance among sites, an effect that we will make explicit in the following when characterizing the associated transition rate.

In addition to the above reactions (2) we here consider the possibility for any selected molecule to diffuse from cell i towards an adjacent cells j. This latter migration can occur only if space allows, namely if cell j has at least one empty case E_j that can be eventually filled. This process can be translated in the following chemical equations [10]:

$$E_j + X_i \xrightarrow{\alpha} E_i + X_j \quad E_i + X_j \xrightarrow{\alpha} E_j + X_i \quad E_j + Y_i \xrightarrow{\beta} E_i + Y_j \quad E_i + Y_j \xrightarrow{\beta} E_j + Y_i, \tag{3}$$

where α and β quantify the ability to diffuse of species X and Y, respectively. The above set of chemical equations define a stochastic model which can be mathematically investigated through the associated master equation. Let us introduce the vectors $\boldsymbol{n} = (\ldots, n_i, \ldots)$ and $\boldsymbol{m} = (\ldots, m_i, \ldots)$. The state of the system is therefore specified by the vector $(\boldsymbol{n}, \boldsymbol{m})$, since the number of empties q_i inside each compartment i can be readily deduced by making use of the conserved quantity (1). The master equation governs the evolution of the probability $P_{\boldsymbol{n},\boldsymbol{m}}(t)$ of seeing the system in the state $(\boldsymbol{n}, \boldsymbol{m})$ at time t. To write down explicitly the master equation, one needs to specify the transition rates associated to the above chemical equations. The transition rate is customarily indicated with the symbol $T(\boldsymbol{n}_F, \boldsymbol{m}_F | \boldsymbol{n}_I, \boldsymbol{m}_I)$, where the index I stands for the initial state and F refers to the final state, compatible with the selected chemical equation. The transition rates that follows reactions (2) can be cast in the form:

$$T(n_i + 1, m_i | n_i, m_i) = a \frac{N - n_i - m_i}{N},$$
$$T(n_i - 1, m_i + 1 | n_i, m_i) = b \frac{n_i}{N},$$
$$T(n_i + 1, m_i - 1 | n_i, m_i) = c \frac{n_i^2}{N^2} \Lambda \sum_{j=-\infty}^{\infty} e^{(-\sigma |i-j|)} \frac{m_j}{N},$$
$$T(n_i - 1, m_i | n_i, m_i) = d \frac{n_i}{N},$$

where we have assumed that the molecules are uniformly distributed inside each mesoscopic cell i. To keep the notation light, we solely keep track of the entries in $\boldsymbol{n}$ and $\boldsymbol{m}$ that get affected by the inspected reaction. The third transition rate encapsulates the long-range coupling to which we alluded above and follows the scheme hypothesized in [6]. The constant σ controls the range of interaction and Λ is a proper normalization constant, to which we will return in the following.

Similarly, the transition rates associated to the diffusion equations (3) read:

$$T(n_i + 1, n_j - 1 | n_i, n_j) = \frac{\alpha}{z} \frac{n_j}{N} \frac{N - n_i - m_i}{N},$$
$$T(n_i - 1, n_j + 1 | n_i, n_j) = \frac{\alpha}{z} \frac{n_i}{N} \frac{N - n_j - m_j}{N},$$
$$T(m_i + 1, m_j - 1 | m_i, m_j) = \frac{\beta}{z} \frac{m_i}{N} \frac{N - n_j - m_j}{N},$$

$$T(m_i-1,m_j+1|m_i,m_j)=\frac{\beta}{z}\frac{m_j}{N}\frac{N-n_i-m_i}{N}.$$

The pair of integers i and j refer to neighbors cells. The factor z stands for the number of nearest neighbors cells: when dealing with a one dimensional system, the case to which we are bound in the forthcoming discussion, $z=2$. Given the above expression for the transition rates, the governing master equation reads:

$$\begin{aligned}\frac{d}{dt}P_{\mathbf{n},\mathbf{m}}(t)=\sum_i\Big[&(\varepsilon^+_{X,i}\varepsilon^-_{Y,i}-1)T(n_i-1,m_i+1|n_i,m_i)\\&+(\varepsilon^-_{X,i}\varepsilon^+_{Y,i}-1)T(n_i+1,m_i-1|n_i,m_i)+(\varepsilon^-_{X,i}-1)T(n_i+1,m_i|n_i,m_i\\&+(\varepsilon^+_{X,i}-1)T(n_i-1,m_i|n_i,m_i)+\sum_{j\in i-1,i+1}\Big((\varepsilon^+_{X,j}\varepsilon^-_{X,i}-1)T(n_i+1,n_j-1|n_i,n_j)\\&+(\varepsilon^+_{X,i}\varepsilon^-_{X,j}-1)T(n_i-1,n_j+1|n_i,n_j)+(\varepsilon^+_{Y,i}\varepsilon^-_{Y,j}-1)T(m_i-1,m_j+1|m_i,m_j)\\&+(\varepsilon^+_{Y,j}\varepsilon^-_{Y,i}-1)T(m_i+1,m_j-1|m_i,m_j)\Big)\Big]P_{\mathbf{n},\mathbf{m}}(t),\end{aligned}\tag{4}$$

where $\varepsilon^\pm_{X,i}$ and $\varepsilon^\pm_{Y,i}$ are the step operators. Assume a generic function $f(\boldsymbol{n},\boldsymbol{m})$. The action of the operator $\varepsilon^\pm_{X,i}$ on $f(\cdot,\cdot)$ is explicited as:

$$\varepsilon^\pm_{X,i}f(\boldsymbol{n},\boldsymbol{m})=f(\ldots,n_i\pm1,\ldots,\boldsymbol{m}).\tag{5}$$

In practical terms $\varepsilon^\pm_{X,i}$ increments or decrements by a unit the population of type X in site i. Similarly, $\varepsilon^\pm_{Y,i}$ acts as specified by the following relation:

$$\varepsilon^\pm_{Y,i}f(\boldsymbol{n},\boldsymbol{m})=f(\boldsymbol{n},\ldots,m_i\pm1,\ldots).\tag{6}$$

The master equation is difficult to handle analytically and one has to resort to approximate techniques of manipulation to progress in the analysis. One viable alternative is the celebrated van Kampen system size expansion, a perturbative calculation that moves from the following working ansatz:

$$\frac{n_i}{N}=\phi_i+\frac{\xi_i}{\sqrt{N}},\quad \frac{m_i}{N}=\psi_i+\frac{\eta_i}{\sqrt{N}}.\tag{7}$$

Consider for instance the number density n_i/N: it is assumed to be split into two independent contributions. ϕ_i is solely function of time and stands for the deterministic concentration as measured in correspondence of the discrete site i. ξ_i is instead a stochastic variable that quantifies the erratic fluctuation that perturbs the idealized mean field (deterministic) solution ϕ_i. The amplitude factor $1/\sqrt{N}$ encodes the finite size of the system and ultimately descends from the central limit theorem. In the limit for infinite systems size, the fluctuations can be neglected and the stochastic system as formulated above converges to its deterministic analogue, $n_i/N\to\phi_i$. Conversely, when working at finite N, stochastic fluctuations do matter and result in sensible deviations from the deterministic description. The role of fluctuations can be quantitatively assessed by carrying out a perturbative calculation based on ansatz (7) and assuming the amplitude factor $1/\sqrt{N}$ to act as a small parameter. The details of the calculation are annexed into the appendices. In the following sections, we shall discuss the results of the analysis, being in particular interested in highlighting the peculiar features that relate to the imposed finite carrying capacity. Next section is entirely devoted to discussing the mean-field limit of model (4).

3 The mean field limit

By truncating the van Kampen system size expansion at the leading order $1/\sqrt{N}$, one eventually obtains the following system of partial differential equations for the deterministic concentrations ϕ_i and ψ_i:

$$\begin{cases} \dfrac{\partial \phi_i}{\partial \tau} = a - a(\phi_i + \psi_i) - (b+d)\phi_i + c\Lambda\phi_i^2 \sum_j \exp(-\sigma|i-j|)\psi_j + \alpha\left(\Delta\phi_i - \psi_i\Delta\phi_i + \phi_i\Delta\psi_i\right), \\ \dfrac{\partial \psi_i}{\partial \tau} = b\phi_i - c\Lambda\phi_i^2 \sum_j \exp(-\sigma|i-j|)\psi_j + \beta\left(\Delta\psi_i - \phi_i\Delta\psi_i + \psi_i\Delta\phi_i\right), \end{cases} \tag{8}$$

where $\Delta f_i = f_{i+1} - 2f_i + f_{i-1}$ is the discrete one dimensional Laplacian and where $\tau = t/N$. Some details of the technicalities involved in the calculation can be found in the annexed Appendix A. Λ is a normalization constant. Following [6] we assign it to match the condition

$$\Lambda \sum_j \exp(-\sigma|j|) = 1,$$

which in turn implies:

$$\Lambda = \frac{e^\sigma - 1}{e^\sigma + 1}.$$

A comment is mandatory at this point. The deterministic model (8) follows from the microscopic stochastic reaction scheme, discussed in the preceding section and it is formally recovered when operating in the thermodynamic limit $N \to \infty$. The effect of the finite carrying capacity imposed in (3), reflects in the mean–field equations through the cross diffusion terms $(-\phi_i\Delta\psi_i + \psi_i\Delta\phi_i)$ which appear to modify the conventional Fickean behaviour. These are second order contributions in the concentrations and are therefore important in the regime of high densities. For this reason, and following the analysis in [10], we believe that Eqs. (8) enables us to extend the analysis of [6] to the interesting regime of crowding conditions. In the remaining part of this paragraph, we will elaborate on the mean field instabilities that can eventually destabilize the homogeneous solution of system (8). In doing so we will adapt the calculation of [6] to the present setting and so identify the peculiarities that can be eventually traced back to the diffusive transport here assumed.

The homogeneous fixed point (ϕ^*, ψ^*) of system (8) is:

$$\phi^* = (a + \sqrt{a^2 - 4ab(a+d)/c})/2/(a+d), \qquad \psi^* = b/c/\phi^*. \tag{9}$$

Impose now a small spatially inhomogeneous perturbation $(\delta\phi_i(t), \delta\psi_i(t))$ to modify the homogeneous fixed point as:

$$\delta\phi_i(t) = \phi_i(t) - \phi^*, \quad \delta\psi_i(t) = \psi_i(t) - \psi^*.$$

We are then interested in identifying the conditions that can yield to a spontaneous amplification of the perturbation and eventually translate in the emergence of Turing or wave like patterns, to which we alluded in the introduction. To this end, and following the standard approach, we solely focus on the linear contributions in $\delta\phi_i$ and $\delta\psi_i$, dropping out higher order corrections. In formulae:

$$\begin{aligned} &\frac{\partial \delta\phi_i}{\partial \tau} - a(\delta\phi_i + \delta\psi_i) - (b+d)\delta\phi_i \\ &= + c\Lambda\phi_i^2 \sum_j \exp(-\sigma|i-j|)\delta\psi_j + 2c\Lambda\psi^*\phi^*\delta\phi_i + \alpha\left(\Delta\delta\phi_i - \psi^*\Delta\delta\phi_i + \phi^*\Delta\delta\psi_i\right), \end{aligned} \tag{10}$$

$$\frac{\partial \delta\psi_i}{\partial \tau} = b\delta\phi_i - c\Lambda\phi_i^2 \sum_j \exp(-\sigma|i-j|)\delta\psi_j + 2c\Lambda\psi^*\phi^*\delta\phi_i + \beta\left(\Delta\delta\psi_i - \phi^*\Delta\delta\psi_i + \psi^*\Delta\delta\phi_i\right). \tag{11}$$

Operate now the spatial Fourier transform of the above system:

$$\begin{aligned}
\frac{\partial \tilde{\delta\phi}}{\partial \tau} &= -a(\tilde{\delta\phi} + \tilde{\delta\psi}) - (b+d)\tilde{\delta\phi} + c\Lambda\tilde{\phi}^2\tilde{e}(k)\tilde{\delta\psi} + 2c\Lambda\psi^*\phi^*\tilde{\delta\phi} + \alpha\left(\tilde{\Delta}\tilde{\delta\phi} - \psi^*\tilde{\Delta}\tilde{\delta\phi} + \phi^*\tilde{\Delta}\tilde{\delta\psi}\right), \\
\frac{\partial \tilde{\delta\psi}}{\partial \tau} &= b\tilde{\delta\phi} - c\Lambda\tilde{\phi}^2\tilde{e}(k)\tilde{\delta\psi} + 2c\Lambda\psi^*\phi^*\tilde{\delta\phi} + \beta\left(\tilde{\Delta}\tilde{\delta\psi} - \phi^*\tilde{\Delta}\tilde{\delta\psi} + \psi^* + \tilde{\Delta}\tilde{\delta\phi}\right),
\end{aligned} \tag{12}$$

where $\tilde{(\cdot)}$ denotes the Fourier transform and $\tilde{\phi} = \tilde{\phi}(k,\tau)$. The two symbols $\tilde{e}(k)$ and $\tilde{\Delta}$ respectively refer to the Fourier transform of the exponential factor in Eqs. (12) and of the discrete Laplacian operator Δ and read:

$$\tilde{\Delta}f(k) = 2[\cos(k) - 1], \qquad \tilde{e}(k) = \frac{\sinh(\sigma)}{\cosh(\sigma) - \cos(k)}.$$

System (12) can be written in a compact form as:

$$\frac{\partial \Psi}{\partial \tau} = J^*(k)\Psi,$$

where $\Psi = (\tilde{\delta\phi}, \tilde{\delta\psi})$ and

$$J^*(k) = \begin{pmatrix} -(b+d) + 2c\phi^*\psi^* - a + \alpha(\tilde{\Delta} - \psi^*\tilde{\Delta}) & c\Lambda(\phi^*)^2\tilde{e}(k) - a + \alpha\phi^*\tilde{\Delta} \\ b - 2c\phi^*\psi^* + \beta\psi^*\tilde{\Delta} & -c\Lambda(\phi^*)^2\tilde{e}(k) + \beta(\tilde{\Delta} - \psi^*\tilde{\Delta}) \end{pmatrix}.$$

The eigenvalues $\lambda_1(k)$ and $\lambda_2(k)$ of matrix $J^*(k)$ provide us with the information concerning the stability of the fixed point to the externally imposed perturbation. Eigenvalues $\lambda_{1,2}$ take the following explicit expression:

$$\lambda_{1,2} = \frac{1}{2}(\mathrm{tr}J^* \pm \sqrt{(\mathrm{tr}J^*)^2 - 4\det J^*}). \tag{13}$$

where $\mathrm{tr}J^*$ and $\det J^*$ stand for the trace and determinant of matrix J^*.

If the real part of both the eigenvalues is negative, for all values of k, the homogeneous state is stable, and the external perturbation gets damped. At variance, if one eigenvalue admits a positive real part, within a compact, finite range of non-zero k, then the perturbation is destabilized and the system undergoes the so–called Turing instability. Beyond the linear regime, non linear terms do matter. Because of the complex and highly non-linear interplay between reaction and diffusion contributions, the system can eventually freeze in asymptotically stationary, non homogeneous configurations. Steady patterns require in addition a null imaginary part of the eigenvalues $\lambda_{1,2}(k)$, for all unstable k values. These are the celebrated Turing patterns, beautiful extended motifs that characterize the stationary distribution of interacting species. Besides the prototypical Turing solution, waves can also manifest when the imaginary part of the eigenvalues is different from zero inside the region of unstable k. In the following, we refer to the dispersion relation $\lambda(k)$ as to the eigenvalue with the largest real part. By studying the function $\lambda(k)$, when varying the parameters of the model, one can elaborate on the conditions that drive Turing and/or waves instabilities. As an example, for demonstrative purposes, we plot in Fig. 1 the dispersion relation $\lambda(k)$ vs. k, for distinct choices of the chemical rate c, having fixed the other parameters to a set of representative values. Interestingly, the profile of $\lambda(k)$ is peaked in $k = \pi$, an important observation that will be extensively used in the following.

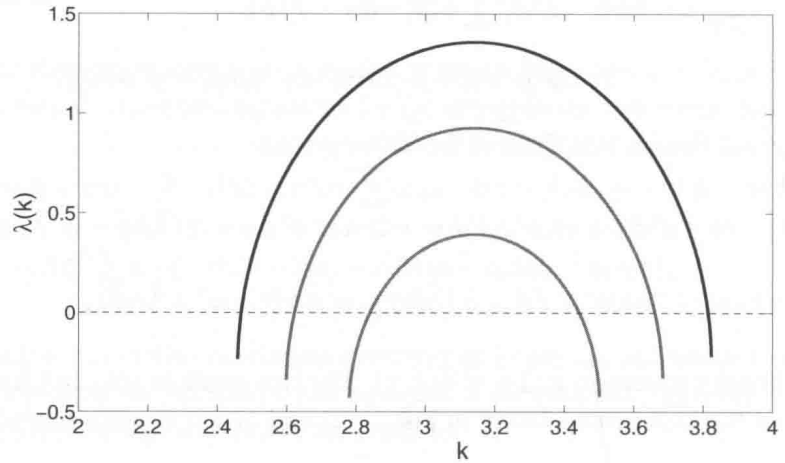

Fig. 1 The dispersion relation $\lambda(k)$ is plotted as a function of the scalar wave number k. The figure refers to $a = d = 1$; $\sigma = 2$; $\alpha = 1; b = 15; \beta = 0.6$. Different curves refer to different values of c: from top to bottom $c = 138, 139, 140$. A finite range of k exists that yield to $\lambda(k) > 0$, so signaling an instability. Notice that the most unstable mode, i.e. the peak of the profile $\lambda(k)$ is located in $k = \pi$.

To discriminate the behaviour of the system, and so classify the possible type of instabilities as reviewed above, we make use of the following general strategy [6, 12, 13]. Clearly, when:

$$\det J^*(k) > 0, \qquad \mathrm{tr}\, J^*(k) < 0 \quad \forall\, k, \tag{14}$$

the fixed point is stable as it can be immediately appreciated by recalling expression (13). When (14) applies, in fact, the real part of $\lambda_i(k)$ is necessarily negative $\forall\, k$. To abandon the region of stability, two different pathways are possible. The transition from stable to unstable solution takes for instance place when there exists a $\bar{k}$ such that $\det J^*(\bar{k}) = 0$ and $\mathrm{tr} J^*(\bar{k}) < 0$, $\forall\, k$. In this case the system enters a region where Turing instability is expected to occur. Another transition realizes when $\mathrm{tr}\, J^*(\bar{k}) = 0$ and $\det J^*(\bar{k}) > 0$, $\forall\, k$, which takes the system into the region of wave instability. Using the above criteria, we can delimit the boundaries of the regions respectively deputed to Turing and wave instability. To favour a pictorial representation of our findings and to make contact with the analysis of [6], we let the (positive) quantities c and β to change freely, and assign the other involved parameters to the values specified in the caption of Fig. 1. The result is displayed in Fig. 2 where three different regions are identified. In region I, waves are predicted to occur, while in region II Turing patterns are expected to develop.When the pair (β, c) falls inside region III, the perturbation fades away and the system relaxes back to the homogeneous solution. Notice that a cusp marks the transition from region II to region III. This bifurcation point (labeled P in Fig. 2) corresponds to the degenerate condition:

$$\det J^*(\bar{k}) = 0, \qquad \mathrm{tr}\, J^*(\bar{k}) = 0, \tag{15}$$

where the scalar $\bar{k}$ identifies the critical wavelength. It is also very interesting to notice that the singular cusp like point occurs at $\beta < 1$, where β measures the diffusion ability of the inhibitor. Recalling, that α, the diffusion coefficient of the activator, is equal to one (see caption of Fig. 2), we conclude that Turing patterns can possibly occur within the explored setting also if $\beta < \alpha$. This is at odd with the customarily agreed scenario, which, it is worth emphasizing, assumes a conventional scheme of diffusion. The cross diffusion terms included in the model here explored to account for the microscopic competition for the finite

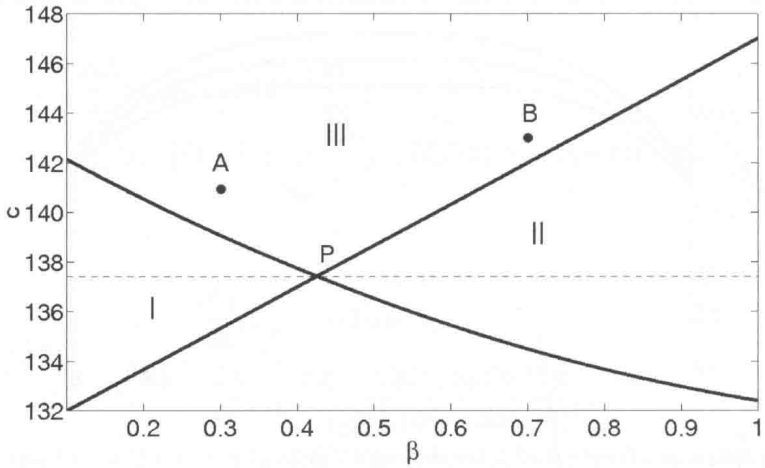

Fig. 2 The regions of wave (labeled with I) and Turing (denoted with II) instabilities are traced in the parameters plane (β,c). Region III identifies the domain of parameters that corresponds to a stable homogeneous fixed point. The other parameters are set as in Fig. 1 and, more specifically, $a = d = 1$, $\sigma = 2$, $\alpha = 1$, $b = 15$. We notice in particular that the Turing instability can occur also when β, the diffusion of the inhibitor, is smaller than $\alpha = 1$, the diffusion of the activator. This observation is at odd with the conventional Turing paradigm and reflects the presence of the cross diffusion terms, in our reaction diffusion scheme. P is positioned in $(\beta_P,\ c_P)$ and identifies the cusp like point where regions I and II touch. The dashed line is horizontal ($c_P = 137.7$) and passes through P. The points A and B fall outside the domain of instability, where the homogeneous fixed point is believed to be stable. As we shall demonstrate later, ordered structures which are reminiscent of wave and Turing like instabilities can develop, driven by stochastic fluctuations, when the parameters are assigned as specified by points A and B of the reference plane (β, c).

spatial resources, are responsible for the observed behaviour, as outlined in [8]. The position of the cusp that separates region II and region III can be used to pinpoint the presence of the Turing order in the classically prohibited region $\beta < \alpha$, or equivalently $\beta < 1$ when $\alpha = 1$, as it is assumed in this paper.

Based on the above, we aim at characterizing analytically, the point of transition from region I and II, by operating in the reference plane (β, c). In this space of reduced dimensionality, two parameters, both β and c, must be varied to force a direct transition from zone I to zone II. For this reason we refer to point P, located in (β_P, c_P), as to a bifurcation. In Figs. 3 and 4 we respectively plot the trace and the determinant of matrix J^* as a function of k, for distinct values of β and for $c = c_P$, a value that we have preliminarily computed numerically. In practice, we cross horizontally the plan (c, β), moving along the dashed line of Fig. 2, which passes from P.

At first glance, from Fig. 3, one sees that the trace of J^* is negatively defined for $\beta > \beta_P$ and, importantly, presents a global maximum in k_M, just before crossing the horizontal axis. The maximum is progressively moved upward when β approaches the critical value β_P. Therefore, it is in $k = k_M$ that the critical condition $\mathrm{tr}\, J^*(k) = 0$ is first matched. Similarly, see Fig. 4, the determinant of $J^*(k)$ is positive for $\beta < \beta_P$ and displays a rather distinct minimum in k_m. By increasing β, the condition $\det J^*(k) = 0$ is reached for the first time in $k = k_m$. This empirical observation defines the starting point of our analysis. Based on the above, we hypothesize in fact that the degenerate condition yielding to the cusp like bifurcation can only occur if: (i) the maximum of the trace and the minimum of the determinant, occur for an identical value of k; (ii) system (15) admits a solution in $k = k_m \equiv k_M$. This latter condition translates in:

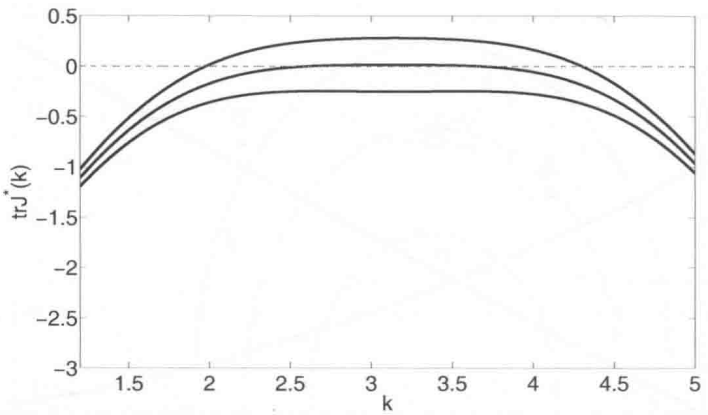

Fig. 3 The trace of J^* is plotted as a function of k, for different values of $\beta = 0.3, 0.42, 0.5$ moving horizontally along the dashed line of Fig. 2, i.e. setting $c = 137.7$. The other parameters are assigned as specified in Fig. 2.

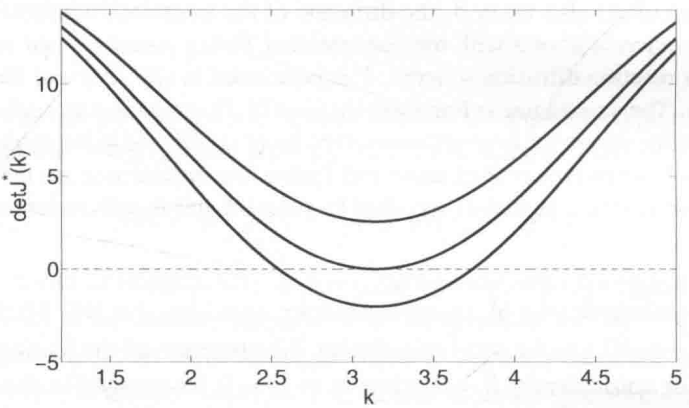

Fig. 4 The determinant of J^* is plotted as a function of k, for different values of $\beta = 0.3, 0.42, 0.5$. For the parameters refer to the caption of Fig. 3.

$$D\tilde{e}(\bar{k}) - E\tilde{e}(\bar{k})\tilde{\Delta} + \tilde{\Delta}^2 F + \tilde{\Delta}G + H = 0, \qquad A + \tilde{\Delta}B - c\Lambda(\phi^*)^2\tilde{e}(\bar{k}) = 0, \tag{16}$$

where

$$\begin{cases} A = -b - d + 2c\phi^*\psi^* - a, \\ B = \alpha(1-\psi^*) + \beta(1-\phi^*), \\ D = c\lambda(\phi^*)^2(d+a), \\ E = c\lambda(\phi^*)^2(\alpha(1-\psi^*) + \beta\psi^*), \\ F = \alpha\beta(1-\psi^*)(1-\phi^*) - \alpha\beta\psi^*\phi^*, \\ G = a\beta\psi^* - \alpha\phi^*(b - 2c\phi^*\psi^*) + \beta(1-\phi^*)(-b-d-a+2c\phi^*\psi^*), \\ H = a(b - 2c\phi^*\psi^*). \end{cases} \tag{17}$$

Condition (i) requires setting to zero the derivative of Eqs. (15) so yielding to the following relations:

$$\begin{cases} \frac{d\tilde{\Delta}}{dk}|_{k=\bar{k}} B - c\Lambda(\phi^*)^2 \frac{d\tilde{e}}{dk}|_{k=\bar{k}} = 0, \\ \frac{d\tilde{e}}{dk}|_{k=\bar{k}} \left(D - E\tilde{\Delta}\right) - \frac{d\tilde{\Delta}}{dk}|_{k=\bar{k}} \left(E\tilde{e}(k) + 2F\tilde{\Delta} + G\right) = 0, \end{cases}$$

where

$$\begin{aligned} \frac{d\tilde{\Delta}}{dk}|_{k=\bar{k}} &= -2\sin(\bar{k}), \\ \frac{d\tilde{e}}{dk}|_{k=\bar{k}} &= \frac{-\sinh(\sigma)\sin(\bar{k})}{(\cosh(\sigma) - \cos(\bar{k}))^2}. \end{aligned} \tag{18}$$

Equations (18) admit a trivial solution when $\bar{k} = n\pi$, with n integer. In fact, both $\frac{d\tilde{\Delta}}{dk}|_{k=n\pi}$ and $\frac{d\tilde{e}}{dk}|_{k=n\pi}$ are identically equal to zero, as it follows from relations (19). For n even, $\tilde{\Delta}(n\pi) = 0$. Under this limiting condition the trace and the determinant collapse to their homologous expressions as obtained for the homogeneous case. Recall that the present calculation builds on a linear expansion around a stable homogeneous fixed point. Therefore, the associated trace and determinant are bound to respectively negative and positive values. In conclusion, conditions (15) cannot be met, if n is assumed to be an even integer.

Conversely, when n is odd, one always gets $\tilde{\Delta}(n\pi) = -4$. Hence, Equations (16) reduce to:

$$\begin{cases} -4B + A - c\Lambda(\phi^*)^2 \frac{\sinh(\sigma)}{\cosh(\sigma)+1} = 0, \\ (D+4E) \frac{\sinh(\sigma)}{\cosh(\sigma)+1} + 16F - 4G + H = 0. \end{cases} \tag{19}$$

System (19) can be solved numerically. It returns the coordinates c_P and β_P of the cusp like point P, as a function of the parameters of the model that enters the definitions of the coefficients implicates in the equations. To favour a pictorial representation of our result, we perform the analysis by tuning continuously b inside a finite interval. We therefore obtain a family of bifurcation points that define a line in the representative parameters plane (β, c). The analysis is then repeated for different choices of σ, as illustrated in Fig. 5.

Our analysis rests on speculative grounds: the mathematical development follows in fact the intuitive idea that the degenerate condition (15) is eventually attained when the stationary points of trace and determinant touch, simultaneously, the horizontal axis. Although reasonable, this working assumption needs to be carefully evaluated. To this end, we turned to computing the exact location of the transition point (β_P, c_P), by delineating for each choice of b the boundaries of the regions respectively deputed to Turing and wave instabilities. The analysis is carried out by setting $\sigma = 1$, for b sampling the aforementioned interval. The results are plotted, with symbols in Fig. 5. The agreement between the (discrete) direct estimates and the (continuous) line based on the analytical strategy implemented above is excellent, thus providing an a posteriori validation of the approximations made. In Fig. 5, we also plot, as a reference, the vertical line $\beta = 1$. When the bifurcation points fall on the left of such line, Turing instability can set in also if the inhibitor diffuses slower than the activator, at odd with the classical scenario which, however, applies to conventional reaction diffusion schemes, where the cross diffusion terms are omitted. If system (19) admits no solutions, then the domains of wave and Turing instabilities appear to be disconnected, as displayed in Fig. 8.

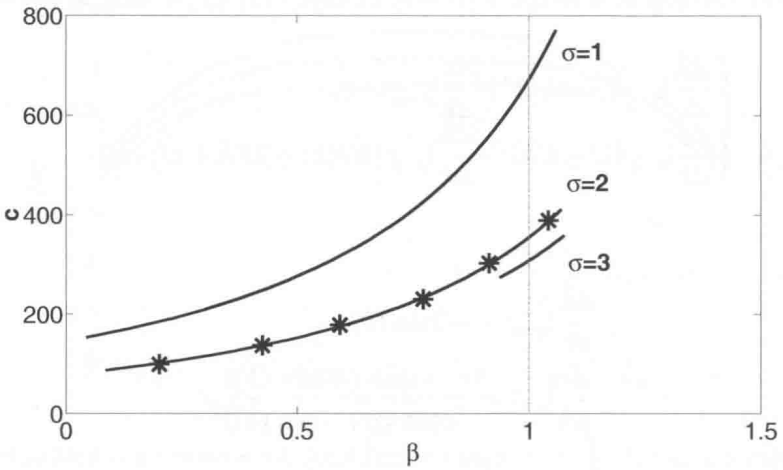

Fig. 5 The bifurcation point (β_P, c_P) as determined by solving system (19) is plotted, for distinct values of σ, and by tuning the parameter b, inside a given interval. Here, $a = d = 1$, $\alpha = 1$ and $\sigma = 1,2,3$. b belongs to the interval $[10,40]$. The symbols (star) refer to direct numerical estimates of the bifurcation points. The agreement between the analytical line and the locations of the bifurcation points as predicted by system (19), constitutes an a posteriori validation of the assumptions made.

As a final remark, we wish to stress that two other stationary points of the dispersion relation can in principle exist, besides the trivial point $k = \pi$. More specifically, two maxima can materialize in $k_\pm$, positions symmetric[a] with respect to $k = \pi$.

We shall return on this interesting observation in the next section when aiming at exploring the impact on the dynamics of the finite size corrections to the idealized deterministic dynamics. As discussed in [7] and [6] Turing patterns and wave can emerge outside the region of mean field order, as follows a self-consistent resonant mechanism that amplifies the endogenous demographic noise. This observation is made quantitative by inspecting analytically the power spectrum of fluctuations and looking for localized peaks both in time and space. These latter peaks testify in fact on the degree of macroscopic organization of the system, as mediated by its granular, hence stochastic, microscopic component.

4 The Stochastic analysis: power spectrum of fluctuations

To the next to leading order in the van Kampen system size expansion, one characterizes the distribution of fluctuations. This latter, labeled $\Pi(\xi,\eta,t)$, obeys to a Fokker Planck equation, which can be equivalently represented in terms of its associated Langevin stochastic equation. Working in this framework, one obtains a close analytical expression for the power spectra of fluctuations $P_i(\omega,k)$, where the index $i = 1,2$ identifies the selected species and k and ω refer to the Fourier time and space frequencies. The details of

[a]Consider Eqs. (18) and focus on the condition $d(\mathrm{tr}J^*)/dk = 0$, more easy to handle. It can be straightforwardly seen that, under specific conditions, two other stationary points $k_\pm$ of the trace J^* exist provided $\left|\cosh(\sigma) - \sqrt{\frac{c\lambda\phi^*\sinh(\sigma)}{2\alpha(1-\psi^*)+2\beta(1-\phi^*)}}\right| < 1$. However, $d(\det J(k)^*)/dk|_{k_\pm} \neq 0$. This implies that the trace maximum and the determinant minimum can simultaneously cross the horizontal axis for the same value of k *only* in $k = \pi$, the value that we considered in the our analysis. In practice, when the above condition is met, and the trace has a maximum in $k_\pm$, the cusp like bifurcation, between Turing and wave regions, cannot realize and a gap opens between those regions in the parameter plane.

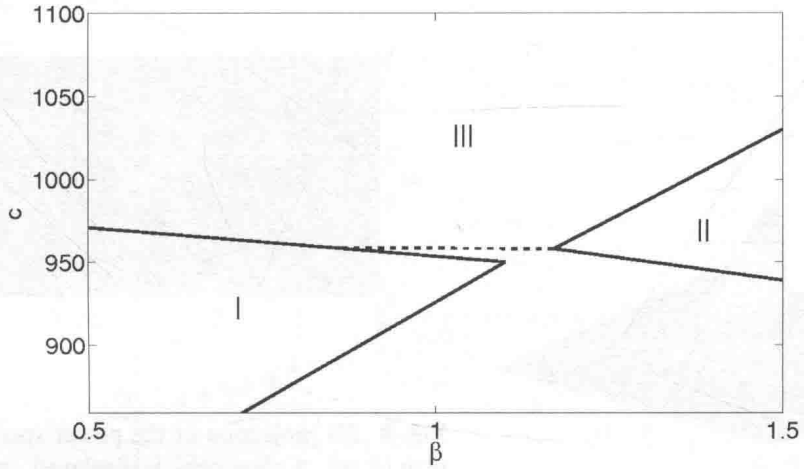

Fig. 6 The regions of wave (I) and Turing (II) instabilities are traced in the parameters plane (β, c), for a choice of b for which system (15) does not admit a solution. As expected the regions I and II appear to be disconnected. III refers to the region of stable homogeneous fixed point. Here, $a = d = 1$, $\alpha = 1$, $\sigma = 2$ and $b = 43$. The dashed line sets the lower boundary of region III. No homogeneous fixed point exists in the portion of plane below the dashed line, and outside the region of Turing and wave instability.

the calculation are confined into the Appendix B, where the expressions for the power spectra are explicitly given, see Eqs. (5). In this section, we exploit this result to represent the computed power spectrum outside the regions of deterministic order. Our aim is to look for the signatures of a spatio-temporal organization, that should ultimately reflects the graininess of the investigated stochastic model. More concretely, we will operate close to the regions of mean field, wave and Turing instabilities, and assign the parameters so to have the system initialized in points A and B, as highlithed in Fig. 2.

The power spectrum relative to position A in the reference plane (β, c) is reported in Figs. 7 and 8. A clear peak is displayed for values of k and ω different from zero. The maximum of the power spectrum is approximately located at $k = \pi$, where the real part of the dispersion has its maximum. Notice that this latter is negative, implying that no instability can develop in the mean field limit. The value that ω takes in correspondence of the peak is very similar to the value that the imaginary part of the dispersion relation has for $k = \pi$, see vertical dashed line in Fig. 8. Stochastic corrections can hence drive the emergence of a quasi-wave, an observation which agrees with the conclusion of [6]. The phase velocity ω/k of the wave can be approximately predicted by working with the linearized mean field equations for the continuum concentration amount. As a simple rule of the thumb, quasi-waves manifest when the system is sufficiently close to region I, i.e. the region of deterministic wave instability, while still being confined in region III, where the homogeneous fixed point is stable.

Conversely, when the parameters are assigned so to fall in the vicinity of region II, stochastic Turing patterns [7] are expected to occur. This intuitive picture finds its justification in Figs. 9 and 10. A localized peak in the power spectrum is in fact seen at $k = \pi$ (the maximum of the real part of the distribution function), along the $\omega = 0$ direction, when the parameters of the system are set to the values corresponding to point B of Fig. 2, just outside the boundaries of the classical Turing region II. Stochastic fluctuations will materialize in a asymptotically stable pattern ($\omega = 0$, namely $t \to \infty$) with a characteristic wavelength that is controlled by the dominant k number. This latter value can be correctly anticipated based on a straightforward linear stability analysis of the underlying deterministic equations.